A kinetic investigation on the synergistic low-temperature reactivity, antagonistic RON blending of high-octane fuels: Diisobutylene and cyclopentane

Hwasup Song, Roland Dauphin, Guillaume Vanhove

A kinetic investigation on the synergistic low-temperature reactivity, antagonistic RON blending of high-octane fuels: Diisobutylene and cyclopentane

Hwasup Song[a], Roland Dauphin[b], Guillaume Vanhove[a,*]

a: Univ. Lille, CNRS, UMR 8522 - PC2A - Physicochimie des Processus de Combustion et de l'Atmosphère, F-59000 Lille, France

b: TOTAL Marketing Services, Centre de Recherche de Solaize, Chemin du Canal – BP 22, 69360 Solaize, France

*Corresponding author: guillaume.vanhove@univ-lille.fr

Full-length article

Abstract

A synergistic effect on low-temperature autoignition reactivity of blending two high-octane compounds, i.e. cyclopentane and diisobutylene, was observed in engine experiments and ignition delay time measurements at 700–880 K and up to 25 bar with a rapid compression machine. Results show that the low-temperature ignition delay and RON of a cyclopentane-diisobutylene blend are inferior to those of its isolated blendstocks, therefore exhibiting an increased reactivity towards ignition at the tested conditions. Sampling and speciation of the reacting mixture during the ignition delay of pure compounds and the most reactive blend was conducted to support discussions focused on the kinetic perspective to this phenomena, which suggest that the separate chain initiation pathways of these potential high-octane blendstocks can interact with each other to help the radical pool growth at the beginning stage of the autoignition chemistry, and finally accelerate the propagation and branching pathways to promote the global reactivity. This result in significant two-stage ignition behavior for the blend, which is not observed at this temperature for both isolated blendstocks. These findings are especially meaningful for designing and blending suitable high-octane fuels for advanced combustion mode engines.

Keywords

Rapid Compression Machine, Blending, Octane Number, Kinetics, Low-Temperature Combustion, Surrogate fuel.

1. Introduction

Today's downsizing trend of spark-ignition (SI) engines requires fuels with superior anti-knock features, to achieve higher thermal efficiency and reduced CO_2 emissions. Using fuels with higher research octane number (RON) and larger octane sensitivity (S), and therefore a lower motor octane number (MON) for a given RON, is found to be beneficial in such operating regimes [1–7]. It is thus an important objective when formulating fuels via the blending of appropriate compounds [8,9].

However, the octane behavior of a blend between two or more compounds is rarely a linear function of the blend composition [10–15]. For example, the octane number of isooctane (iC8) – ethanol blends increases steeply as the ethanol content increases at low ethanol composition, but shows a saturated behavior as more ethanol is blended [16]. In this case, it has been proven that the superior latent heat of vaporization of ethanol cools down the fuel-air mixture dramatically, therefore affecting the global reactivity of the in-cylinder mixture, through what is called evaporative charge cooling. However, such a non-linear octane number blending behavior is not always induced by the physical properties of fuel, but in some cases has a kinetic origin. Leppard focused on the non-linear octane blending behavior of small olefins with primary reference fuels (PRF), which consist of iC8 and *n*-heptane, by extensive engine experiments and speciation [17]. 2-Butene and 1,3-butadiene were selected because of their similar RON to iC8. It was suggested that reaction pathways specific to olefins compete with that of the PRF components to slow down the global reactivity of the blend at the lowest temperatures, while the opposite was true at higher temperatures. In case of larger olefins such as diisobutylene (DIB, a mixture of 2,4,4-trimethyl-1-pentene, i.e. DIB-1, and 2,4,4-trimethyl-2-pentene, i.e. DIB-2), which has a RON superior to 100 and a larger S about 17, the synergistic octane-boosting effect of DIB-1 with iC8 was observed in engine experiments [13]. In another study, DIB was blended with PRFs and fueled into an engine, and the unburned mixture was sampled to investigate the modification of the reaction pathways induced by DIB addition [18]. Similar efforts were also conducted using different high octane compounds, for example

Dauphin et al. [15] examined the effect of the composition of mixtures of cyclopentane (CPT) and aromatics blended into iC8 and observed synergistic octane boosting effect. Fundamental combustion research facilities, i.e. a shock tube (ST) and a rapid compression machine (RCM) were used to elucidate this effect from a chemical kinetics perspective. In the process, it was concluded that the ignition delay times (IDT) measured at 1000 K in a shock tube showed a linear relationship with MON. On the other hand, the IDTs measured in an RCM in the low-to-intermediate temperature conditions, and exhibiting two-stage ignition behavior, were not in a linear correlation against RON. This was explained by taking into account the comparably shorter residence time of the engine unburned gas in the engine with comparison to the RCM IDT. Furthermore, the strong coupling between first-stage heat release and second-stage ignition delay probably renders such correlations irrealistic.

Most of these previous studies focused on the non-linear octane blending behavior of mixtures of a non-octane sensitive fuel (such as PRF) and an octane sensitive compound (such as an alkene or an aromatic). However, conventional transport fuels usually consist of various hydrocarbons classes, and their contents are generally regulated. Interactions of the reaction pathways specific to classes of octane-sensitive compounds could thus take place, and impact the global reactivity of the blended fuel. In addition to that, while most of the non-linear octane blending was realized and studied using an internal combustion engine, in which the thermodynamic state of the fuel-air mixture evolves rapidly during the engine cycle, utilizing a dedicated device for fundamental combustion studies is advantageous to isolate the kinetic aspects of non-linear octane blending behavior. This endeavor was the primary motive for this study, where two octane-sensitive and widely used blendstocks, namely CPT and DIB, were selected and blended with iC8.

Table 1 provides some important characteristics of CPT and DIB. CPT is considered as a major component of FACE gasolines [19,20], and recent kinetic modeling efforts [21,22] have improved the knowledge of its low-to-intermediate temperature combustion kinetics. Generally speaking, CPT is less reactive with regards to ignition than *n*-pentane over the low-to-intermediate temperature regime. It is

suggested that this results mostly from higher energy barriers for the internal isomerization pathways RO_2 -> QO_2H , which in the case of CPT proceed through the formation of bicyclic transition states [21]. This favors an alternative reaction pathway leading to the formation of olefins and HO_2, which does not directly lead to chemical branching, hence lowering the global reactivity. In the case of DIB which has a structural similarity to iC8, recent work on DIB-1 and DIB-2 proposes a comprehensive oxidation model based on experimental measurements from a wide variety of facilities as well as ab initio calculations and mechanism construction [23]. From another perspective focused on exhaust gas composition, single cylinder engine experiments were also conducted with DIB and the effect of equivalence ratio was studied [24]; other previous works include a low-temperature kinetic model based on jet-stirred reactor (JSR) experiments [25], a high-temperature study from a theoretical chemistry approach [26,27], shock tube experiments [28,29], and laminar flame speed measurements [30]. Some of these studies are however specific to only one of the two isomers [24–27,29].

Table 1. Fuel properties

	iC8	CPT	DIB
RON	100	103.1*	102.1*
MON	100	86.1*	85.4*
Lower heating value [MJ/kg]	44.310	44.636	43.998

***: this study.**

The main objective of this study is to investigate the effect of chemical interaction between CPT and DIB specific reaction pathways under engine-relevant conditions in which the unburned gas autoignition is closely related to the engine knock phenomena, by means of an extensive RCM experimental study, including ignition delay measurements and investigation of the formed stable intermediate species, as well as RON measurements.

2. Experimental setup

IDTs of binary and ternary blends featuring iC8, CPT, and DIB were measured with the ULille rapid compression machine (RCM), which has already been used on numerous studies of the low-to-intermediate temperature combustion kinetics of hydrocarbons. Only a brief explanation of the experimental apparatus is given here, hence the readers are encouraged to look for more details from the historical bibliography [31,32].

The mixture inside the combustion chamber is compressed in 45 ms by a driven piston, which is propelled by a pneumatically-operated driving piston via a right angle metal cam element, this particular coupling allowing suppression of potential driven piston rebound after the compression, and good reproducibility of the compression phase. The combustion chamber is preheated by electric elements, with a less than 1 K temperature deviation along the axial direction at bottom dead center. A creviced piston [33] is used to absorb the developing thermal boundary layer mass during the compression and suppress potential piston corner roll-up vortex, which can promote temperature inhomogeneity across the combustion chamber if not handled accordingly [32,34]. The pressure history throughout the experiment was acquired by a piezoelectric transducer protected from thermal shock (Kistler 601CA) and a charge amplifier (Kistler 5007). The adiabatic core assumption was assumed to compute the compressed core gas temperature T_C, which is varied by modifying the inert gas composition using mixtures of N_2 and Ar, while keeping the mixture equivalence ratio at 1.0 and the inert-to-oxygen ratio of 3.76:1. Reactants were prepared in glass vessels following the partial pressure method and using iC8 (>98.0%, Sigma-Aldrich), CPT (>96%, Merck), DIB (mix of 74 v/v% DIB-1 and 21 v/v% DIB-2, impurities < 5%, TOTAL Marketing & Services) and gases (>99.99%, Air Liquide). An uncertainty of 5 K is assumed for the compressed gas temperature [35]. For the pure components, i.e. iC8 and CPT, repeated freeze-thaw distillation were conducted to remove any eventual dissolved gases within their flasks, while the DIB mixture was injected with a syringe by carefully matching the required amount of DIB to reach the

desired partial pressure. IDT is defined as the elapsed time between the end of the compression and the moment where the pressure rise rate is at its maximum value, as depicted in Fig. 1. Also provided in the same figure is a non-reacting pressure profile which helps to distinguish a pre-ignition heat release, if any, by comparing with the reacting pressure profile. Non-reacting mixtures are prepared by replacing the O_2 fraction of the reacting mixture with N_2. All of the ignition delay experiments were performed a minimum of three times, all of the results being shown in the Figures. Tables of the experimental results and non-reacting pressure profiles are included in the Supplementary Material.

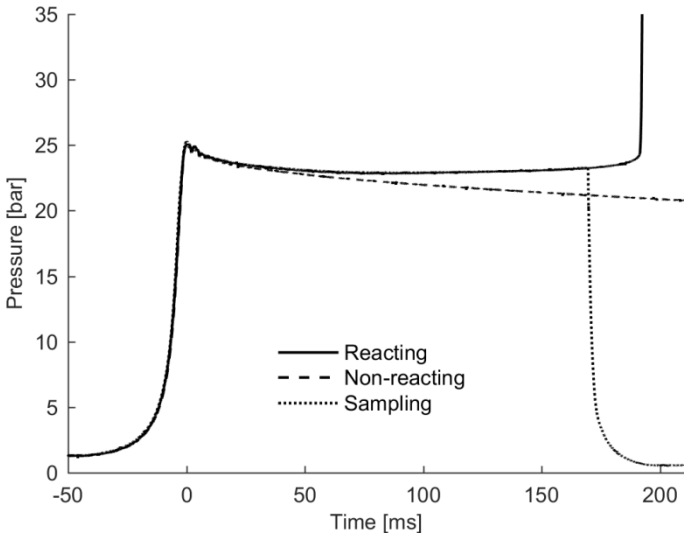

Fig. 1. Experimental pressure profiles obtained from the ULille RCM. Reactant mole fractions: DIB/O_2/N_2 = 0.01721/0.2065/0.7763 at Tc = 700±1 K, Pc = 25±0.3 bar.

To gain insight on the low-temperature combustion kinetics of these blended fuels, the reacting mixture inside the combustion chamber was sampled during the ignition delay period and analyzed with a gas chromatography/mass spectrometry (GC/MS) bench to quantify and identify the stable intermediate species which are formed during the ignition delay period. Such an experimental approach is also useful to develop kinetic models and/or assess the model validity, as demonstrated for example in a recent 2,5-dimethyltetrahydrofuran study [31]. Sampling is realized through expansion of the compressed gas into a dedicated sampling canister, with a volume ratio between the combustion chamber and the canister of

over 40 times. This allows immediate quenching of the reactivity, with a time required for the pressure to drop below 50% of its initial value of less than 1 ms, as demonstrated in Fig. 1.

The acquired samples are then injected into a primary GC (Bruker Scion 456-GC) equipped with a thermal conductivity detector (TCD), a flame ionization detector (FID) and MS, and BR-5 and Bond-Q columns for separating larger and smaller organic compounds, and a GC (Agilent 6890) equipped with a molecular sieve and TCD/FID detectors for measuring CO, small hydrocarbons and permanent gases.

The Research Octane Number (RON) measurements were carried out on a standard CFR engine. The CFR engine is a 2-valve 4-stroke single cylinder spark ignition engine with specific features allowing varying the compression ratio from 4.5:1 to 18:1 by moving the cylinder height. The engine is connected to an electric synchronous motor that maintains a constant rotational speed (600 rpm). The CFR engine is equipped with a 4-bowl variable-level carburettor supplying the fuels to the engine. This configuration allows a fast alternation between the tested fuel and the two reference PRFs (Primary Reference Fuels) without stopping the engine as required in the ASTM standard procedure [36].

3. Results and Discussion

3.1. IDTs at RON-like condition

The IDTs of all blending components were measured at a core gas temperature of T_C = 700±1.5 K and two different top dead center (TDC) pressures of p_C = 25±0.18 bar and 20±0.17 bar, which are close to "RON-like" condition as discussed in the literature [1,15,37], while keeping the equivalence ratio at unity. Finally, for a total of 21 different ternary blends, whose blending composition was varied by 20 mol. % steps, were tested and their IDTs are depicted in Fig. 2 on a ternary diagram. Given that at least 3 repeated experiments were conducted under a same condition, the averaged IDT values were used for this diagram. It should be noted that while all these experiments were conducted during a brief period of time,

reproducibility tests were conducted after a period of months, and yielded identical results. For the binary blends of iC8/CPT and iC8/DIB, a monotonic evolution of the IDT can be observed as the concentration evolves, while the CPT/DIB blend shows a synergistic effect on the global reactivity, as its IDT is shorter than any of its base compound. In this work, we describe synergistic or antagonistic behavior in the point of view of reactivity, as opposed to the point of view of knock resistance. It can be noted that at the p_C = 20 bar condition, the maximum measured IDTs are superior to the commonly accepted limit for RCM IDT reporting of 200 ms. We however chose to report this data as the results were found to be reproducible within 2.3 ms with the longest IDTs, the trends similar at 20 and 25 bar, and because these data do not impact the conclusions of the synergistic effect on the reactivity. Kinetic modeling of these very long ignition delay times with standard 0D-procedures should not however be expected to reach full agreement.

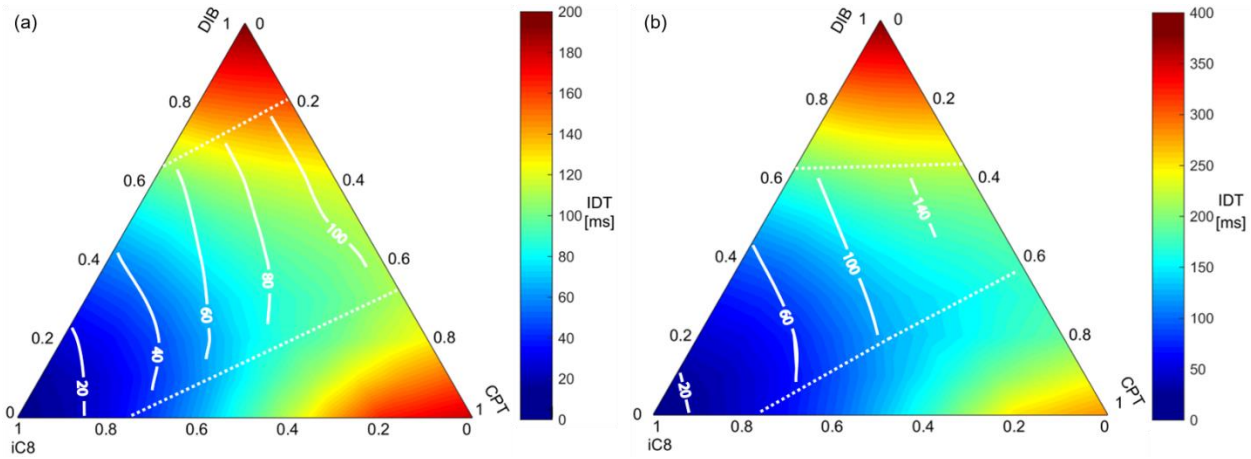

Fig. 2. IDT diagrams of the iC8/CPT/DIB ternary blend at 700 K and different TDC pressures of (a) 25 bar and (b) 20 bar. White dashed lines indicate the boundary of the two-stage ignition occurrence, along with the white contour lines which show the first stage ignition delay times. Note that the maximum range of the color bars is different in two diagrams.

The non-filtered pressure profiles of various blends at the TDC condition of 700 K and 25 bar are depicted in Fig. 3, where the typical low-temperature oxidation behavior of different hydrocarbon classes are also observed: Isooctane exhibits the shortest IDT combined with a first-stage ignition coupled with

an intense low-temperature heat release typical of long chain alkanes, while a weak and gradual low-temperature heat release was observed for DIB, coupled with a long IDT, as demonstrated by comparing unreactive and reactive pressure profiles in Fig. 1. This gradual low-temperature heat release is typical of short alkyl chain alkenes, as already demonstrated for example for 3-hexene [38]. For CPT, recent studies point out the existence of a negative temperature coefficient (NTC) behavior [22], as observed for other cycloalkanes [39]. Two-stage ignition behavior is however not as distinct for cycloalkanes as it is for alkanes, and was not observed for CPT at this 700K condition. In the case of the iC8/DIB and iC8/CPT mixtures, smooth transition from two-stage ignition to single-stage ignition is observed as the iC8 content is reduced, as seen from Figs. 3(a) and 3(b). However, in the case of the DIB/CPT binary mixtures, while both pure blendstocks initially display single-stage ignition, two-stage ignition can be observed from roughly 20% to 60% CPT, as depicted in Fig.3(c), and the shortest total IDT being observed for the 60/40 CPT/DIB blend. This specific phenomenon is consistent throughout the ternary blends as iC8 is added, e.g. the IDT of iC8/CPT/DIB = 60/20/20 blend is shorter than those of the 60/40/0 and the 60/0/40 blends (compare Figs.3(a), 3(b), and 3(d)).

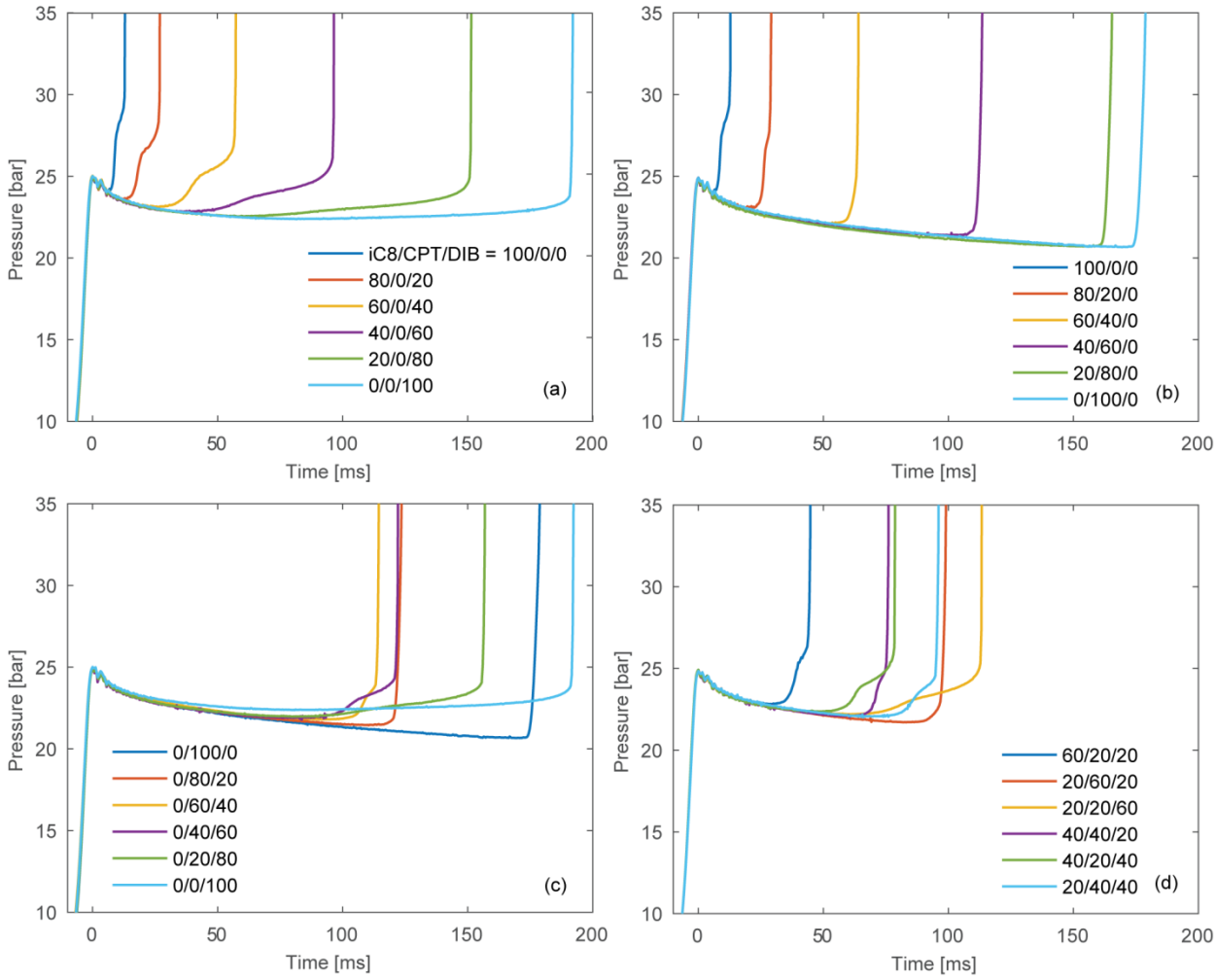

Fig. 3. Pressure profiles of the blends during their ignition delay period. (a) iC8 and DIB binary, (b) iC8 and CPT binary, (c) CPT and DIB binary, and (d) all-containing ternary blend.

The synergistic effect on the reactivity of CPT/DIB blend was confirmed from RON measurements with a CFR engine, as presented in Fig. 4. Here, the effect of blending CPT and DIB is therefore slightly "antagonistic" from the RON perspective, as a minimum RON is measured with a 50/50 (wt%) blend. The antagonistic effect is however below the reproducibility level agreed by the method at this high RON measurement level; to avoid too high uncertainties in the measurement process, all the measurements were performed in a raw, allowing to improve the interval of confidence of the measurements, as can be stated by the rather good alignment of the experimental data forming a smooth curve. The antagonistic

effect stated on RON is in good agreement with the IDT measurements, where the shortest IDT is observed with the 60/40 (mol%) blend that is almost equivalent to 50/50 (wt%, i.e. 61.5/38.5 (mol%)).

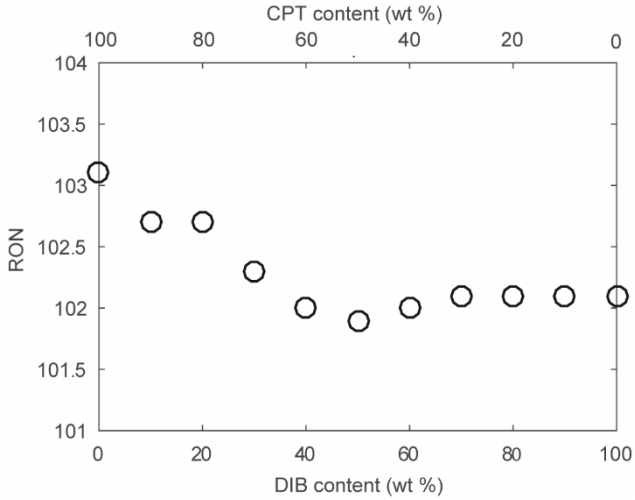

Fig. 4. Measured RONs for CPT/DIB mixtures.

3.2. Full IDT curves over low-to-intermediate temperatures

IDTs between 700 and 880 K for CPT, DIB and the CPT/DIB = 60/40 (mol%) blend (called "60/40 blend" hereafter for simplicity) were measured to gain more insight on the synergistic effect over a low-to-intermediate temperature range, and compared as depicted in Fig. 5. Again, all the experiments were repeated 3 times under a same initial condition to see the repeatability and all of the obtained data are presented in Fig. 5. Comparison with the available literature on CPT shows that the measured IDTs are in good agreement with the existing data [22], the ignition delays measured for this study being slightly longer than observed in previous work from another RCM, mostly over the NTC region. The synergistic effect on reactivity is again obvious, as the IDTs of 60/40 blend is shortest at the lowest temperatures, i.e. below 730 K. This is consistent with the observation of first-stage ignition only in the case of the 60/40 blend, this first-stage heat release leading to a lower total ignition delay. As temperature increases, the IDTs of the 60/40 mixture lie in between those of DIB and CPT. The overall IDT curve can be split into

three zones regimes; below 730 K where the blend is the most reactive, between 730 and 770 K where the 60/40 blend IDT curve is closest to the CPT IDT curve, and above 770 K where 60/40 blend IDT curve is closest to the DIB IDT curve. On a first approximation, these findings infer that the governing kinetics for the ignition of the blend are imposed by DIB for temperatures above 770 K, and by CPT for temperatures between 730 and 770 K. In the following sections of this manuscript, detailed attention will be devoted to gain insight into the kinetic reasons for the synergistic behavior observed at the lowest temperatures, by means of sampling of the reacting mixture during the IDT.

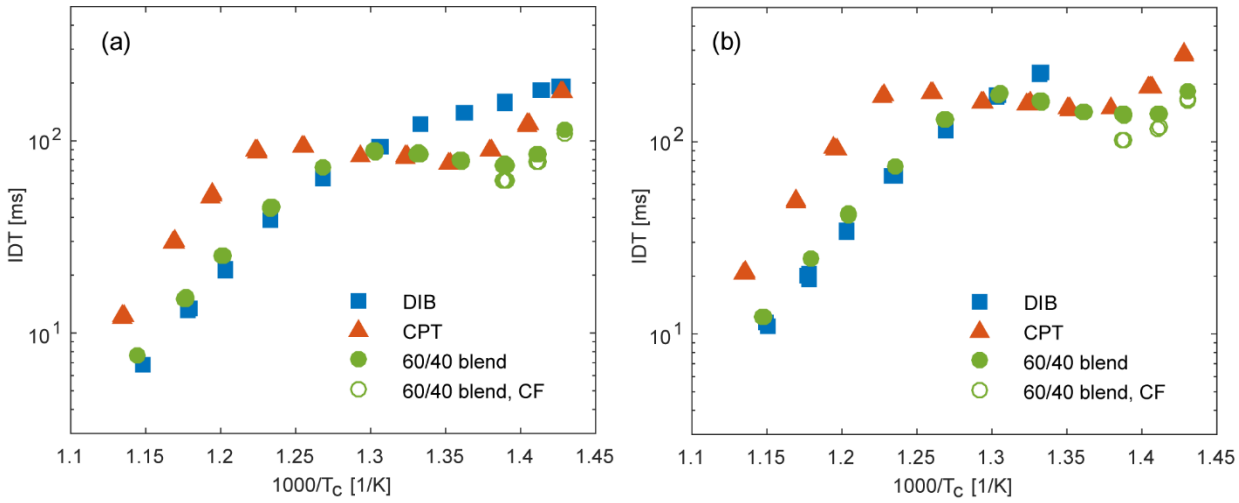

Fig. 5. IDT curves of the base components and the 60/40 blend at the TDC pressure of (a) 25 bar and (b) 20 bar. 1st stage IDTs, whenever measurable, are also presented.

3.3. Intermediate species sampling

As described in Section 2, sampling experiments are conducted to identify and quantify the stable intermediate species formed during the ignition delay period, for all three fuels at the T_C = 700 K, p_C = 25 bar condition. Mole fractions of the quantified species were obtained by using the effective carbon number (ECN) method to estimate the calibration factors [40], and the quantification uncertainty was estimated to ±15%, which is typical in a GC system and which accounts for the estimation uncertainties of the calibration factors using the ECN. It should be noted that since most of the discussion relies on

comparisons between the observed mole fractions for products between the different initial fuels, the values of the calibration factors do not influence the conclusions, and the uncertainty for the comparisons could probably be lowered to less than 10%. While running the GC, an identical temperature program was applied to directly compare the quantities of the common intermediate species from each fuel. In this way detecting any fuel-specific intermediate species is also easier and intuitive. In the case of DIB, samples were obtained between 0.88–0.92 of the normalized ignition delay time, i.e. between 169.5–176.3 ms (where the average IDT was 193 ms), to compare with samples obtained from the 60/40 blend at 103.8–105.9 ms (with an average IDT of 114.6 ms). In the case of CPT, samples were obtained between 0.79–0.82 of the normalized ignition delay period, i.e. between 141.8–146.4 ms (with the average IDT being 179.6 ms). This timing was chosen to compare with pre-cool flame speciation results of the 60/40 blend taken at 90.8 ms and 90.9 ms, which also correspond to ~0.8 of the normalized ignition delay period. Detailed information of the identified species is provided as supplementary material.

3.3.1. Major intermediate species formed before DIB ignition

Most of the experimentally observed intermediate species correspond well with the results from the kinetic modeling study of pure DIB isomers, DIB-1 and DIB-2, which is also based on the experimental speciation from the authors' group [23].

3.3.1.1. Unimolecular decomposition

Considering the bond dissociation energies of DIB-1 and DIB-2 [30], isobutene can be directly formed in large amounts, amongst other reaction pathways, after a C-C scission between the quaternary and the secondary carbon of DIB-1. Therefore, smaller intermediate species originating from isobutene oxidation pathways are also experimentally observed, but not all of their formation pathways are discussed in this work. Readers can refer to the comprehensive kinetic modeling study of isobutene [41] for more details. Another unimolecular decomposition product is 2,4-dimethyl-1,3-pentadiene (24-diMeC5-13diene), which comes after the loss of a methyl radical from the quaternary carbon of DIB-2. Note that the

formation of these species can also take place after the formation of a non-allylic alkenyl radical and O_2 addition, followed by the loss of HO_2.

3.3.1.2. OH-addition to the double bond

Direct OH radical addition to a double bond and following O_2 addition leads to the formation of two aldehydes or ketones via the so-called Waddington mechanism [42]. Applying this to DIB isomers explains the formation of 4,4-dimethyl-2-pentanone (44diMe2C5-one) and formaldehyde (for DIB-1), acetone, and 2,2-dimethylpropanal (22diMe-ProAl, for DIB-2), as shown in Fig. 6. The formation of acetone can also take place through the Waddington mechanism on isobutene. It has to be noted that formaldehyde, however observed in the MS chromatograms, was not quantified.

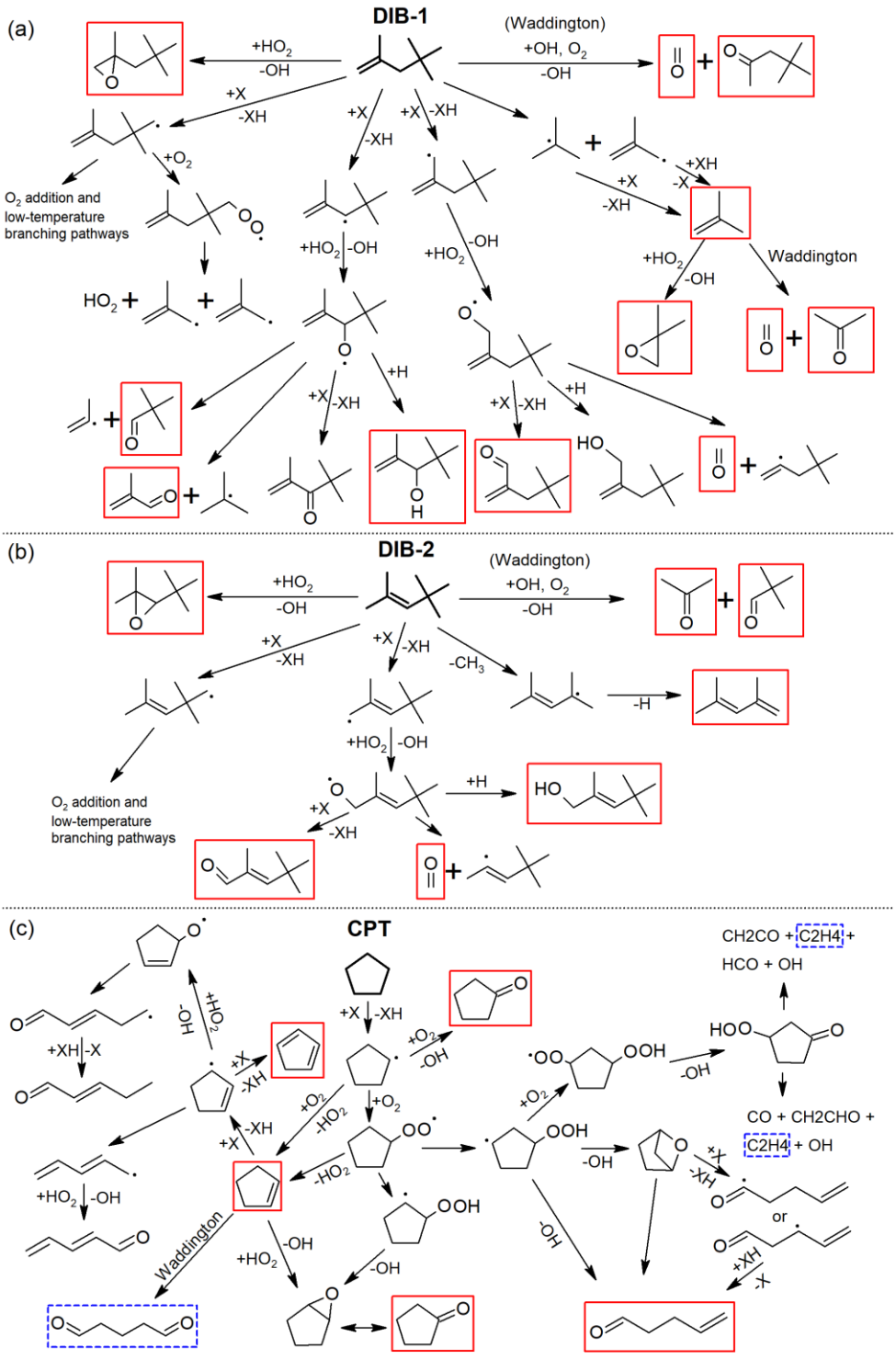

Fig. 6. Low-temperature reaction pathways of DIB-1 (a), DIB-2 (b) and CPT (c). Experimentally identified species from pure components and the 60/40 blend are highlighted with red boxes. Blue dashed boxes indicate species that were observed only for the 60/40 blend case.

3.3.1.3. HO_2 addition to the double bond

Another double bond-specific reaction pathway is the addition of a HO_2 radical to a double bond, which leads to the formation of an alkylic QO_2H, which often decomposes into an oxirane and an OH radical. This type of reaction, while not being a chain branching pathway, leads to an increase of the global reactivity by converting an HO_2 radical into an OH radical [38,43–45]. The HO_2 addition product of DIB-1 is therefore 2-methyl-2-neopentyloxirane (2Me2NeoC5yl-Oxi), while that of DIB-2 is 2-*tert*-butyl-3,3-dimethyloxirane (2tByl33diMe-Oxi), as described in Fig. 6(a) and (b). The formation of 2,2-dimethyloxirane from isobutene is also expected from this reaction pathway.

3.3.1.4. HO_2 addition to the allylic diisobutenyl radicals

In the case of alkenes, H abstraction to form an allylic alkenyl radical is preferential with regards to other sites. The addition of such radicals to O_2 is not favored as it would for alkanes [46], due to the significantly lower activation energy barrier of the backward reaction involving an alkenyl radical R,

$R + O_2 \rightarrow RO_2$ (Eq. 1)

and hence the backwards decomposition of RO_2 is facilitated. Instead, as previously described in alkene kinetic modeling studies [38,44], the addition of HO_2 radical on the allylic alkenyl radical usually results in $HO_2 \rightarrow$ OH conversion through a chemically activated pathway, as described in [47]. At the pressures and temperatures of interest here, however, it is likely that the resulting QOOH adduct will also be stabilized to the hydroperoxide, before potentially forming a carbonyl and H_2O. While the chemically-activated pathway will facilitate reactivity by producing two very active radicals, the formation of the hydroperoxide can also delay the ignition process via added degenerate chain branching, therefore resulting in a sink for HO_2 radicals. For the DIB isomers, the formation of 4,4-dimethyl-2-methylenevaleraldehyde (44diMe2Mln-C5Al), propene, 2,2-dimethylpropanal, 2-methyl-2-propenal (methacrolein), 2,4,4-trimethyl-1-penten-3-ol (244triMeC5-1en-3ol), 2,4,4-trimethyl-2-pentenal

(244triMeC5-2enAl), and 2,4,4-trimethyl-2-penten-1-ol (244triMeC5-2en-1ol) can thereby take place as depicted in Fig. 6(a) and (b).

3.3.2. Major intermediate species formed before CPT ignition

The formation of most of the identified intermediate species can be explained by the recent CPT kinetic model [22], which was constituted adopting the typical O_2 addition and following low-temperature chain branching scheme of alkanes. At lower temperatures, after the first H abstraction and the addition of the resulting cyclopentyl radical on O_2, the fate of the cyclopentylperoxy radical is either to follow an internal isomerization step of RO_2 → QOOH as for long chain alkanes [22,48], or forming cyclopentene (CyC5H8) along with an HO_2 radical. For cyclopentene, this can also be formed via a formally direct, chemically-activated channel of R + O_2 → R// + HO_2 [45]. Based on a reaction path analysis conducted at 700 K and 20 atm in this CPT kinetic modeling study [22], i.e. close to the experimental condition investigated in the current work, the isomerization to QOOH corresponds to 26.6% of cyclopentyl radical consumption, compared to 61.0% for the cyclopentene formation pathways, mostly because of the higher potential energy barriers towards the isomerization channel.

3.3.2.1. Species after internal isomerization of RO_2 → QOOH

As presented in Fig. 6(c), isomerization is possible from two independent sites; one at the alpha carbon adjacent to the peroxy group, and the other at the beta carbon. While 1,2-epoxycyclopentane is expected after the H transfer from the alpha carbon, this was not experimentally measured in our conditions. Instead, a small amount of cyclopentanone (CyC5-one) was quantified by an order of ppm. Following the possible isomerization reaction converting an oxirane into a ketone [49], cyclopentanone could be a marker of the formation of 1,2-epoxycyclopentane; however, another possibility of cyclopentanone formation from the cyclopentyl radical addition to O_2 also needs to be considered, as shown in Fig. 6(c).

Internal isomerization from the beta carbon leads to a second O_2 addition and the following low-temperature chain branching to ketohydroperoxide formation. The decomposition of such a

ketohydroperoxide will form several species including ethylene as major detectable intermediate species during first-stage ignition. However, ethylene was not observed from the sampling experiments at a sampling timing of 0.8 times the ignition delay, and no evidence of low-temperature heat release and corresponding first-stage ignition behavior was observable in the pure CPT experimental pressure profiles at 700 K, while a mild low-temperature heat release during the induction period was expected from the simulation at the same condition using the current CPT kinetic model [22], similar to the case depicted in Fig.1. The absence of ethylene, along with very small detected quantities of 4-pentenal (C5-4enAl) and cyclopentanone—on the order of ppm—suggests that the internal H atom transfer pathways are not as fast as suggested by the current model, and that further improvements to the current CPT model might be necessary.

3.3.2.2. Further reactivity of cyclopentene

The facilitated H abstraction from the two allylic carbons of cyclopentene facilitate the formation of 1,3-cyclopentadiene (13-CyC5H6) as well as 2-pentenal or 2,4-pentadienal after scission of the C5 ring, or 1,5-pentanedial through the Waddington mechanism, as shown in Fig. 6(c). Direct HO_2 addition on the double bond will also lead to 1,2-epoxycyclopentane and eventually cyclopentanone, as previously discussed. However, their quantities are below the detection limit for pure CPT.

3.3.3. Major intermediate species formed before the 60/40 blend ignition

Most of the species found from the 60/40 blend correspond with the results from the aforementioned DIB and CPT sampling results, however some intermediate species were detected only from the 60/40 blend—1,5-pentanedial (glutaraldehyde, C5-15diAl), ethylene, 1-butene, ethyloxirane, and propanal—to name a few. Possible reasons for their formation could be either an unveiled chemical interaction between CPT and DIB, or that the existence of either CPT or DIB drives the chain branching of the other component under the low-temperature combustion regime.

Interestingly, the relative formation of the DIB-originated intermediate species, which is calculated by normalizing their mole fractions with respect to the initial DIB mole fraction, changes for certain species groups discussed in Section 3.3.1. On the other hand, the formation of the CPT-originated intermediate species is promoted when compared to the pure CPT case, implying that the low-temperature oxidation chemistry of DIB facilitates the reactions involving CPT and its products, which will be discussed later. This is also demonstrated by looking into the conversion of each fuel compounds, as the DIB conversion rate decreases from about 23% (pure DIB at ~0.9 normalized IDT) to 4% (pre-cool flame of 60/40 blend at ~0.8 normalized IDT) and 13% (post-cool flame of 60/40 blend at ~0.9 normalized IDT), while that of CPT increases from around 2% (pure CPT at ~0.8 normalized IDT) to 4% (pre-cool flame of 60/40 blend at ~0.8 normalized IDT) and 12% (post-cool flame of 60/40 blend at ~0.9 normalized IDT). Figure 7 presents the comparison of relative quantities of the major intermediate species exhibiting important changes of the low-temperature reaction pathway of DIB.

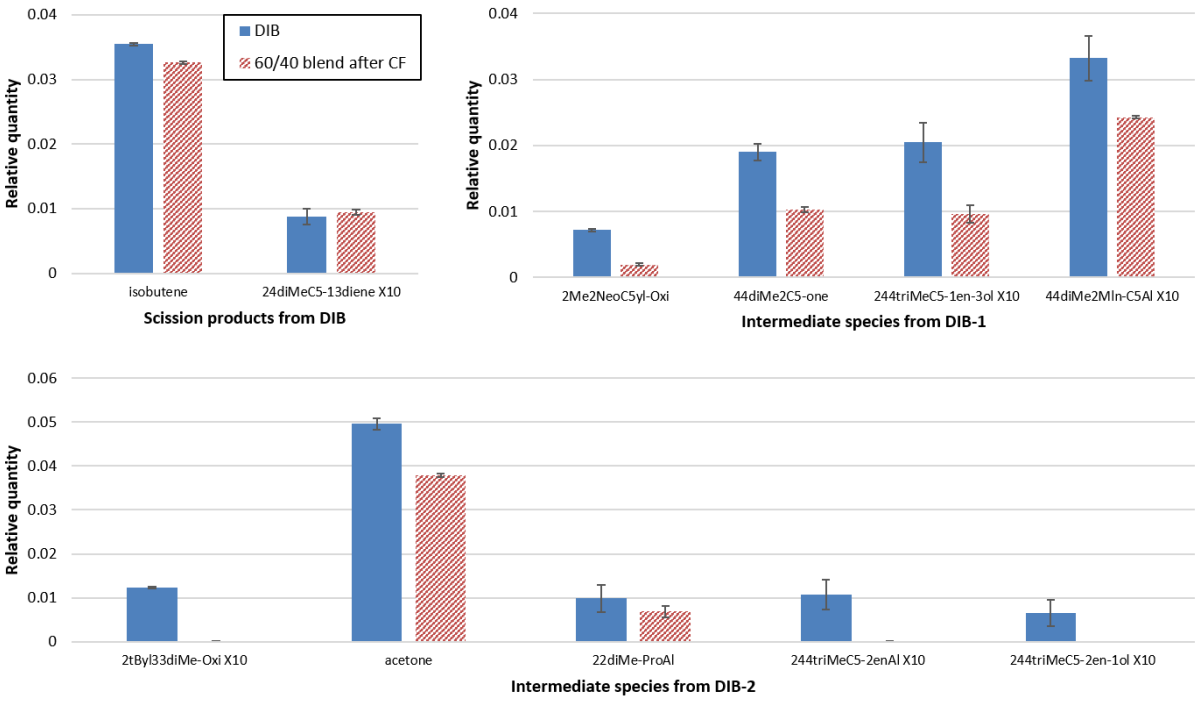

Fig. 7. Relative quantities of selected intermediate species normalized by the initial DIB mole fraction. Blue solid bar: results from DIB, red hatched bar: results from 60/40 blend after the cool flame. Error bars indicate the 1σ-standard deviation of the results from at least 3 repeated experiments on both fuels.

3.3.3.1. HO_2 addition to the double bond and to the allylic diisobutenyl radicals

The formation of HO_2 adducts of DIB isomers, i.e. 2-methyl-2-neopentyloxirane and 2-*tert*-butyl-3,3-dimethyloxirane, is dramatically affected by the presence of CPT as seen in Fig.7. The relative quantity of 2-methyl-2-neopentyloxirane from the 60/40 blend is less than one third to the DIB case. Moreover, 2-*tert*-butyl-3,3-dimethyloxirane does not appear, implying that HO_2 radicals are less consumed via the DIB reaction pathways. This is consistent with other reaction pathways involving HO_2, especially the HO_2 addition on the allylic diisobutenyl radicals and the resultant intermediate species such as 4,4-dimethyl-2-methylenevaleraldehyde, 2,4,4-trimethyl-1-penten-3-ol, 2,4,4-trimethyl-2-pentenal, and 2,4,4-trimethyl-2-penten-1-ol.

While the HO_2 participation to the DIB low-temperature chain branching is reduced, it is likely that CPT benefits from an increased contribution of HO_2 to the initiation of its own low-temperature branching pathways. In detail, the HO_2 addition pathway on the allylic cyclopentenyl radical is promoted, which leads to the formation of 2-pentenal and 4-pentenal [22]. Comparison with the CPT mole fraction data, both before and after the first-stage ignition event observed for the blend, shows that the relative quantity of 4-pentenal increases significantly in the case of the blend, as depicted in Fig. 8, which could also explain the synergistic blending effect as this pathway promotes the global reactivity by converting HO_2 into OH. The reduced contribution of HO_2 to the formation of the hydroperoxide after addition to allylic diisobutenyl radicals also possibly reduces the HO_2 sink effect resulting from the degenerate chain-branching, and described in 3.3.1.4. Along with that, the quantity of cyclopentanone in the 60/40 blend case before the low-temperature heat release is already larger than the CPT-only case at a similar timing of 0.8 times the IDT, and after the cool-flame event the amount increases by almost an order, which is also a meaningful increment as the formation of cyclopentanone is accompanied by HO_2 → OH conversion, as well as promoted OH production from the reactivity resulting from the cyclopentyl radical addition to O_2.

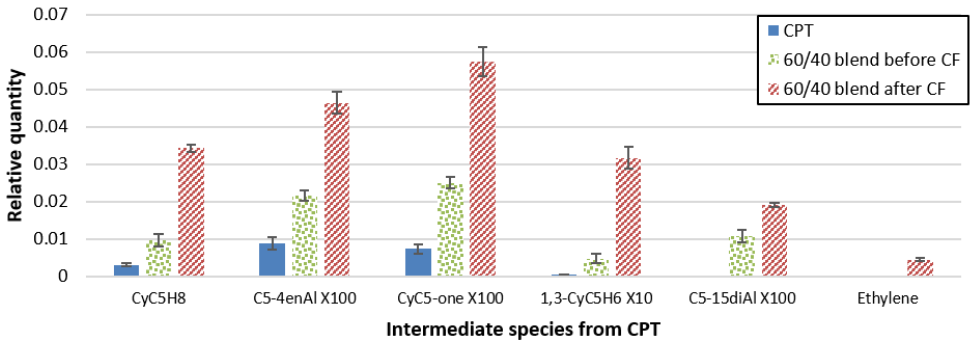

Fig. 8. Relative quantities of the CPT-derived intermediate species, normalized by the initial mole fraction of CPT. Blue solid bar: results from CPT, green dotted bar: results from 60/40 blend prior to the low-temperature heat release, red hatched bar: results from 60/40 blend after the low-temperature heat release.

3.3.3.2. OH addition to the double bond

The relative quantities of aldehydes and ketones produced from DIB-1 and DIB-2 after the Waddington mechanism, i.e. 4,4-dimethyl-2-pentanone, acetone, and 2,2-dimethylpropanal, also decrease as shown in Fig. 7. On the other hand, the Waddington product from cyclopentene, i.e. 1,5-pentanedial, is observed from the 60/40 blend, which contrasts with the pure CPT case. This can be explained as a result of faster OH pool development from both the HO_2 → OH conversion as well as the stimulated low-temperature chain branching of CPT itself.

3.3.3.3. Unimolecular decomposition

Unlike other DIB intermediate species, the relative quantities of unimolecular decomposition products from DIB isomers, i.e. isobutene and 2,4-dimethyl-1,3-pentadiene, remain almost unchanged in the blending case, as shown in Fig.7. Combined with the other experimental observations, it may be concluded that HO_2, which is a representative reaction chain carrier for the low-temperature combustion, is the major cause for the synergistic, reactivity-promoting blending of DIB with CPT, probably due to the easier H abstraction from the allylic carbons of the DIB isomers and therefore more chance of HO_2 formation than the pure CPT case, and the occurrence of reaction steps that convert HO_2 into OH. The C-H bond dissociation energies from the primary and secondary allylic carbons of the DIB isomers are within the range of 94.1–95.8 kcal/mol [30], compared to 96.9 kcal/mol of CPT [50]. It should also be noted that the relative quantities of cyclopentene and 1,3-cyclopentadiene prior to the cool-flame occurrence from the 60/40 blend, are already larger than in the pure CPT case, at a similar sampling time relative to ignition. At later times, after first-stage ignition, the formation of CPT-relevant intermediate species is even more accelerated.

3.3.3.4. CPT ketohydroperoxide decomposition

A number of intermediate species, most of which are smaller hydrocarbons, were observed after first-stage ignition in the 60/40 blend case. Among them, ethylene is expected from the decomposition of the

ketohydroperoxide originating from CPT [22]; hence, even though it could originate from other pathways, it could be an indicator that the proposed CPT low-temperature chain branching reactions proceed faster in the 60/40 blend case than in the pure CPT case under the same compressed condition. We propose the conclusion that this is observable mostly because of the stimulated H-abstraction from CPT as previously discussed.

3.3.3.5. Miscellaneous products

1-butene is formed after the cool-flame outbreak, which corresponds to the detection of 1-butene at the lower temperature limit around 840 K from a JSR experimental study of isobutene [51]. It could also be formed from ring opening reactions from cyclopentane sub-chemistry. Furthermore, ethyloxirane appears as an HO_2 adduct of 1-butene, and propanal as a Waddington product. 2-butene can also be produced from 1-butene after the resonance stabilization, but its relatively larger quantity is unexpected and further investigation is necessary.

3.4. Elucidating the enhanced reactivity from relevant reaction rates

To the authors' knowledge, none of the published kinetic models including both CPT and DIB sub-mechanisms, for example [52], can reproduce this synergistic effect at the low temperature condition. Merging the DIB model [23] and the recent CPT model [22] also didn't allow the reproduction of the experimental results from this study. Nevertheless, a speculative discussion based on the reaction rates is presented to provide some insight on the temperature-dependent synergistic effect from a kinetics perspective. All the relevant rate coefficients were taken from a recent CPT comprehensive model [22] and the up-to-date DIB isomers model [23], including H-abstraction by HO_2 and OH radicals on the allylic, alkylic, and vinylic carbons from DIB-1 and DIB-2, H-abstraction by HO_2 and OH radicals from CPT, and HO_2 and OH additions on DIB-1 and DIB-2.

Figure 9 presents the relative branching fractions of H-abstraction and radical addition reactions on CPT and DIB isomers. The order of magnitude of the reaction rate constants involving HO_2 grows rapidly from ~10^7 (600 K) to ~10^{10} (900 K) [$cm^3 \cdot mol^{-1} \cdot s^{-1}$], while the rate constants involving OH are ~10^{13} $cm^3 \cdot mol^{-1} \cdot s^{-1}$ over the whole temperature range of interest, thus less sensitive to the temperature. For H-abstractions by O_2, rate constants range from ~10^{-2} to ~10^3 $cm^3 \cdot mol^{-1} \cdot s^{-1}$ between 600–900 K for DIB, whereas ~10^{-4} to ~10^2 $cm^3 \cdot mol^{-1} \cdot s^{-1}$ within the same temperature range for CPT. Results show that the branching fraction of HO_2 on the H-abstraction from CPT is nearly constant, while the maximum value is about 39.8% near 760 K. Compared to this, the branching to the H-abstraction from DIB isomers continuously increases as temperature increases, however the value is about 43.8% at 700 K, which is similar to the CPT case and hence the H-abstraction reactions from DIB and CPT by HO_2 are competing at lower temperatures. On the other hand, H-abstraction by O_2 is strongly favored on DIB to form HO_2 in comparison to CPT as seen from Fig. 9, which implies that that the chain initiation relative to CPT and further HO_2 → OH conversion is facilitated . This effect could also be enhanced by the slight exothermicity accompanying the major DIB reaction pathways, and which results in slight heat release along the ignition delay, as observed in the pressure profiles (see Figs. 1 and 3c). Once this occurs, the low temperature combustion kinetics of CPT are accelerated, facilitating the occurrence of 1st stage ignition.

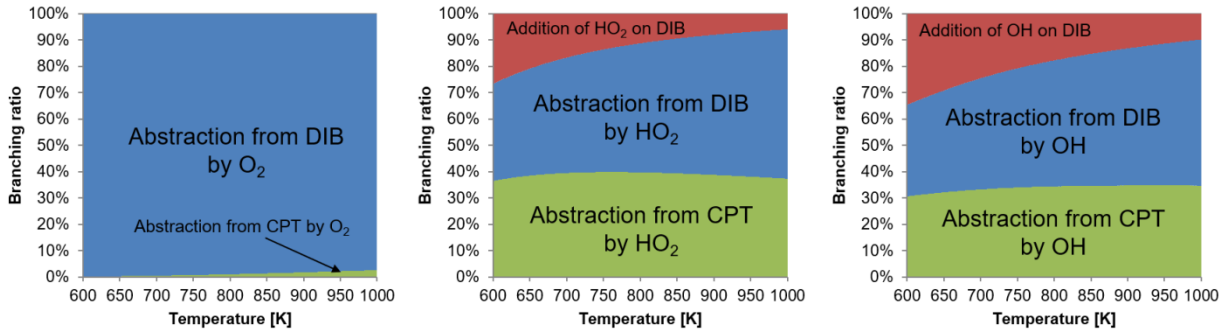

Fig. 9. Branching fractions of chain initiation by radicals and O_2.

4. Conclusions

Synergistic blending behavior of promoting the global reactivity has been demonstrated in the case of blends of CPT and DIB through the measurement of IDTs at a fixed compressed temperature of 700 K of various iC8/CPT/DIB blends, RON measurements of the CPT/DIB blends, and low-to-intermediate temperature IDT measurements of pure compounds and the CPT/DIB binary blend in the ULille RCM. A thorough investigation on the oxidation kinetics of the blend is conducted by speciation of the reacting mixture. The following conclusions can be drawn:

- Under high pressure and low temperature conditions relevant to boosted SI engines, the global reactivity of a ternary iC8/CPT/DIB blend is promoted with the presence of CPT and DIB at the same time, as demonstrated by IDT and RON measurements.
- The synergistic blending behavior is observed at all temperatures below 720 K, which emphasizes the role of low-temperature combustion reaction pathways of CPT and DIB.
- Speciation and quantification of the intermediates formed by pure CPT and DIB, as well as the blend show that the presence of DIB, and its HO_2 -> OH conversion pathways is initiating the low-temperature chain branching of CPT.
- Results imply that when formulating future fuels for an advanced, turbocharged SI engine, kinetic interactions between potential fuel blendstocks need to be tested and considered to avoid any undesirable, antagonistic RON changes.

We propose the following explanation to the observed synergistic behavior observed between CPT and DIB:

- H- abstraction by O_2 is strongly favored on DIB, and forms HO_2.
- HO_2 can react to form OH by adding to the double bond, and undergoes slightly exothermic reactivity, while initiating CPT reactivity as well.

- OH can take part into the LTC kinetics of CPT with the help of increased temperature, resulting in a 1st stage ignition event.
- Temperature increases during this process, and brings the mixture into the intermediate temperature regime, where DIB ignition delay is inferior to CPT.

Acknowledgements

This research was funded by TOTAL Marketing Services and is a contribution to the CPER research project Climibio. HS and GV thank the Région Hauts-de-France, and the Ministère de l'Enseignement Supérieur et de la Recherche (CPER Climibio), and the European Fund for Regional Economic Development for their financial support.

Supplementary materials

Experimental data (IDT, pressure profiles, relative formation data)

References

[1] J.P. Szybist, D.A. Splitter, Understanding chemistry-specific fuel differences at a constant RON in a boosted SI engine, Fuel. 217 (2018) 370–381. https://doi.org/10.1016/j.fuel.2017.12.100.
[2] K.P. Somers, R.F. Cracknell, H.J. Curran, A chemical kinetic interpretation of the octane appetite of modern gasoline engines, Proc. Combust. Inst. 37 (2019) 4857–4864. https://doi.org/10.1016/j.proci.2018.05.123.
[3] M. Kassai, C. Aksu, T. Shiraishi, R. Cracknell, M. Shibuya, Mechanism Analysis on the Effect of Fuel Properties on Knocking Performance at Boosted Conditions, in: SAE Technical Paper 2019-01-0035, 2019. https://doi.org/10.4271/2019-01-0035.
[4] R. Cracknell, W. Warnecke, J.-H. Redmann, T.K. Goh, Octane requirements of modern downsized boosted gasoline engines, MTZ Worldw. 76 (2015) 4–7.

[5] G.T. Kalghatgi, Fuel Anti-Knock Quality - Part I. Engine Studies, in: SAE Technical Paper 2001-01-3584, 2001. https://doi.org/10.4271/2001-01-3584.
[6] G.T. Kalghatgi, Fuel Anti-Knock Quality- Part II. Vehicle Studies - How Relevant is Motor Octane Number (MON) in Modern Engines?, in: SAE Technical paper 2001-01-3585, 2001. https://doi.org/10.4271/2001-01-3585.
[7] G.T. Kalghatgi, K. Nakata, K. Mogi, Octane Appetite Studies in Direct Injection Spark Ignition (DISI) Engines, in: SAE Technical Paper 2005-01-0244, 2005. https://doi.org/10.4271/2005-01-0244.
[8] D. Kim, C.K. Westbrook, A. Violi, Two-stage ignition behavior and octane sensitivity of toluene reference fuels as gasoline surrogate, Combust. Flame. 210 (2019) 100–113. https://doi.org/10.1016/j.combustflame.2019.08.019.
[9] M.D. Boot, M. Tian, E.J. Hensen, S.M. Sarathy, Impact of fuel molecular structure on auto-ignition behavior–Design rules for future high performance gasolines, Prog. Energy Combust. Sci. 60 (2017) 1–25.
[10] V. Knop, M. Loos, C. Pera, N. Jeuland, A linear-by-mole blending rule for octane numbers of n-heptane/iso-octane/toluene mixtures, Fuel. 115 (2014) 666–673.
[11] N. Rankovic, G. Bourhis, M. Loos, R. Dauphin, Understanding octane number evolution for enabling alternative low RON refinery streams and octane boosters as transportation fuels, Fuel. 150 (2015) 41–47. https://doi.org/10.1016/j.fuel.2015.02.005.
[12] N. Morgan, A. Smallbone, A. Bhave, M. Kraft, R. Cracknell, G. Kalghatgi, Mapping surrogate gasoline compositions into RON/MON space, Combust. Flame. 157 (2010) 1122–1131.
[13] R.L. Bradow, M. Alperstein, Analytical investigations of isooctane and diisobutylene slow combustion in an Otto-cycle engine, Combust. Flame. 11 (1967) 26–34.
[14] T.M. Foong, K.J. Morganti, M.J. Brear, G. da Silva, Y. Yang, F.L. Dryer, The octane numbers of ethanol blended with gasoline and its surrogates, Fuel. 115 (2014) 727–739.
[15] R. Dauphin, J. Obiols, D. Serrano, Y. Fenard, A. Comandini, L. Starck, G. Vanhove, N. Chaumeix, Using RON Synergistic Effects to Formulate Fuels for Better Fuel Economy and Lower CO2 Emissions, in: SAE Technical Paper 2019-01-2155, 2019. https://saemobilus.sae.org/content/2019-01-2155/.
[16] E. Kasseris, J.B. Heywood, Charge cooling effects on knock limits in SI DI engines using gasoline/ethanol blends: Part 1-quantifying charge cooling, in: SAE Technical Paper 2012-01-1275, 2012. https://doi.org/10.4271/2012-01-1275.
[17] Leppard, William R., The autoignition chemistries of primary reference fuels, olefin/paraffin binary mixtures, and non-linear octane blending, in: SAE Technical Paper 922325, 1992. https://doi.org/10.4271/922325.
[18] D. Kang, S. Kirby, J. Agudelo, M. Lapuerta, K. Al-Qurashi, A.L. Boehman, Combined Impact of Branching and Unsaturation on the Autoignition of Binary Blends in a Motored Engine, Energy Fuels. 28 (2014) 7203–7215. https://doi.org/10.1021/ef501629p.
[19] S.M. Sarathy, G. Kukkadapu, M. Mehl, T. Javed, A. Ahmed, N. Naser, A. Tekawade, G. Kosiba, M. AlAbbad, E. Singh, S. Park, M.A. Rashidi, S.H. Chung, W.L. Roberts, M.A. Oehlschlaeger, C.-J. Sung, A. Farooq, Compositional effects on the ignition of FACE gasolines, Combust. Flame. 169 (2016) 171–193. https://doi.org/10.1016/j.combustflame.2016.04.010.
[20] S.M. Sarathy, A. Farooq, G.T. Kalghatgi, Recent progress in gasoline surrogate fuels, Prog. Energy Combust. Sci. 65 (2018) 67–108. https://doi.org/10.1016/j.pecs.2017.09.004.

[21] M.J. Al Rashidi, M. Mehl, W.J. Pitz, S. Mohamed, S.M. Sarathy, Cyclopentane combustion chemistry. Part I: Mechanism development and computational kinetics, Combust. Flame. 183 (2017) 358–371. https://doi.org/10.1016/j.combustflame.2017.05.018.
[22] M.J. Al Rashidi, J.C. Mármol, C. Banyon, M.B. Sajid, M. Mehl, W.J. Pitz, S. Mohamed, A. Alfazazi, T. Lu, H.J. Curran, A. Farooq, S.M. Sarathy, Cyclopentane combustion. Part II. Ignition delay measurements and mechanism validation, Combust. Flame. 183 (2017) 372–385. https://doi.org/10.1016/j.combustflame.2017.05.017.
[23] N. Lokachari, G. Kukkadapu, H. Song, H.J. Curran, G. Vanhove, W.J. Pitz, A comprehensive experimental and kinetic modeling study on diisobutylene oxidation, (in preparation).
[24] J.S. Ninomiya, A. Golovoy, Use of Diisobutylene Fuel in a Single Cylinder Engine: Effects of Equivalence Ratio on Exhaust Composition, J. Air Pollut. Control Assoc. 19 (1969) 879–883. https://doi.org/10.1080/00022470.1969.10469353.
[25] G. Yin, Z. Gao, E. Hu, Z. Xu, Z. Huang, Comprehensive experimental and kinetic study of 2,4,4-trimethyl-1-pentene oxidation, Combust. Flame. 208 (2019) 246–261. https://doi.org/10.1016/j.combustflame.2019.07.008.
[26] G. Yin, E. Hu, X. Li, J. Ku, Z. Gao, Z. Huang, Theoretical Study of Abstraction and Addition Reactions of 2,4,4-Trimethyl-1-pentene with H and O(^{3}P) Radical, Energy Fuels. 32 (2018) 11831–11842. https://doi.org/10.1021/acs.energyfuels.8b01917.
[27] G. Yin, E. Hu, Z. Gao, F. Yang, Z. Huang, Kinetics of H abstraction and addition reactions of 2,4,4-trimethyl-2-pentene by OH radical, Chem. Phys. Lett. 696 (2018) 125–134. https://doi.org/10.1016/j.cplett.2018.02.024.
[28] W.K. Metcalfe, W.J. Pitz, H.J. Curran, J.M. Simmie, C.K. Westbrook, The development of a detailed chemical kinetic mechanism for diisobutylene and comparison to shock tube ignition times, Proc. Combust. Inst. 31 (2007) 377–384. https://doi.org/10.1016/j.proci.2006.07.207.
[29] E. Hu, G. Yin, Z. Gao, Y. Liu, J. Ku, Z. Huang, Experimental and kinetic modeling study on 2,4,4-trimethyl-1-pentene ignition behind reflected shock waves, Fuel. 195 (2017) 97–104. https://doi.org/10.1016/j.fuel.2017.01.055.
[30] G. Yin, E. Hu, S. Huang, J. Ku, X. Li, Z. Xu, Z. Huang, Experimental and kinetic study of diisobutylene isomers in laminar flames, Energy. 170 (2019) 537–545. https://doi.org/10.1016/j.energy.2018.12.194.
[31] Y. Fenard, H. Song, H. Minwegen, P. Parab, C. Sampaio Mergulhão, G. Vanhove, K.-A. Heufer, 2,5-Dimethyltetrahydrofuran combustion: Ignition delay times at high and low temperatures, speciation measurements and detailed kinetic modeling, Combust. Flame. 203 (2019) 341–351. https://doi.org/10.1016/j.combustflame.2019.02.022.
[32] Goldsborough, S. Scott., Hochgreb, Simone., Vanhove, Guillaume., Wooldridge, Margaret S., Curran, Henry J., Sung, Chih-Jen, Advances in rapid compression machine studies of low- and intermediate-temperature autoignition phenomena, Prog. Energy Combust. Sci. 63 (2017) 1–78. https://doi.org/10.1016/j.pecs.2017.05.002.
[33] D. Lee, S. Hochgreb, Rapid Compression Machines: Heat Transfer and Suppression of Corner Vortex, Combust. Flame. 114 (1998) 531–545.
[34] N. Bourgeois, S.S. Goldsborough, H. Jeanmart, F. Contino, CFD simulations of Rapid Compression Machines using detailed chemistry: Evaluation of the 'crevice containment' concept, Combust. Flame. 189 (2018) 225–239. https://doi.org/10.1016/j.combustflame.2017.10.033.

[35] B.W. Weber, C.-J. Sung, M.W. Renfro, On the uncertainty of temperature estimation in a rapid compression machine, Combust. Flame. 162 (2015) 2518–2528. https://doi.org/10.1016/j.combustflame.2015.03.001.
[36] Standard Test Method for Research Octane Number of Spark Ignition Engine Fuel, (D2699).
[37] M. Mehl, T. Faravelli, F. Giavazzi, E. Ranzi, P. Scorletti, A. Tardani, D. Terna, Detailed Chemistry Promotes Understanding of Octane Numbers and Gasoline Sensitivity, Energy Fuels. 20 (2006) 2391–2398. https://doi.org/10.1021/ef060339s.
[38] G. Vanhove, M. Ribaucour, R. Minetti, On the influence of the position of the double bond on the low-temperature chemistry of hexenes, Proc. Combust. Inst. 30 (2005) 1065–1072. https://doi.org/10.1016/j.proci.2004.08.042.
[39] O. Lemaire, M. Ribaucour, M. Carlier, R. Minetti, The production of benzene in the low-temperature oxidation of cyclohexane, cyclohexene, and cyclohexa-1, 3-diene, Combust. Flame. 127 (2001) 1971–1980.
[40] J.T. Scanlon, D.E. Willis, Calculation of Flame Ionization Detector Relative Response Factors Using the Effective Carbon Number Concept, J. Chromatogr. Sci. 23 (1985) 333–340. https://doi.org/10.1093/chromsci/23.8.333.
[41] C.-W. Zhou, Y. Li, E. O'Connor, K.P. Somers, S. Thion, C. Keesee, O. Mathieu, E.L. Petersen, T.A. DeVerter, M.A. Oehlschlaeger, G. Kukkadapu, C.-J. Sung, M. Alrefae, F. Khaled, A. Farooq, P. Dirrenberger, P.-A. Glaude, F. Battin-Leclerc, J. Santner, Y. Ju, T. Held, F.M. Haas, F.L. Dryer, H.J. Curran, A comprehensive experimental and modeling study of isobutene oxidation, Combust. Flame. 167 (2016) 353–379. https://doi.org/10.1016/j.combustflame.2016.01.021.
[42] Ray, D.J.M, Redfearn, A., Waddington, D.J., Gas-phase oxidation of alkenes: decomposition of hydroxy-substituted peroxyl radicals, J. Chem. Soc. Perkin Trans. 2 (1973) 540–543.
[43] M. Mehl, G. Vanhove, W.J. Pitz, E. Ranzi, Oxidation and combustion of the n-hexene isomers: A wide range kinetic modeling study, Combust. Flame. 155 (2008) 756–772. https://doi.org/10.1016/j.combustflame.2008.07.004.
[44] J. Zádor, S.J. Klippenstein, J.A. Miller, Pressure-Dependent OH Yields in Alkene + HO_2 Reactions: A Theoretical Study, J. Phys. Chem. A. 115 (2011) 10218–10225. https://doi.org/10.1021/jp2059276.
[45] J. Zádor, C.A. Taatjes, R.X. Fernandes, Kinetics of elementary reactions in low-temperature autoignition chemistry, Prog. Energy Combust. Sci. 37 (2011) 371–421. https://doi.org/10.1016/j.pecs.2010.06.006.
[46] F. Battin-Leclerc, Detailed chemical kinetic models for the low-temperature combustion of hydrocarbons with application to gasoline and diesel fuel surrogates, Prog. Energy Combust. Sci. 34 (2008) 440–498. https://doi.org/10.1016/j.pecs.2007.10.002.
[47] C.F. Goldsmith, S.J. Klippenstein, W.H. Green, Theoretical rate coefficients for allyl+HO2 and allyloxy decomposition, Proc. Combust. Inst. 33 (2011) 273–282. https://doi.org/10.1016/j.proci.2010.05.054.
[48] M.J. Al Rashidi, S. Thion, C. Togbé, G. Dayma, M. Mehl, P. Dagaut, W.J. Pitz, J. Zádor, S.M. Sarathy, Elucidating reactivity regimes in cyclopentane oxidation: Jet stirred reactor experiments, computational chemistry, and kinetic modeling, Proc. Combust. Inst. 36 (2017) 469–477. https://doi.org/10.1016/j.proci.2016.05.036.

[49] A. Lifshitz, C. Tamburu, Isomerization and Decomposition of 2,3-Dimethyloxirane. Studies with a Single-Pulse Shock Tube, J. Phys. Chem. 99 (1995) 10251–10260. https://doi.org/10.1021/j100025a028.
[50] Z. Tian, A. Fattahi, L. Lis, S.R. Kass, Cycloalkane and cycloalkene C− H bond dissociation energies, J. Am. Chem. Soc. 128 (2006) 17087–17092.
[51] P. Dagaut, M. Cathonnet, Isobutene Oxidation and Ignition: Experimental and Detailed Kinetic Modeling Study, Combust. Sci. Technol. 137 (1998) 237–275. https://doi.org/10.1080/00102209808952053.
[52] G. Kukkadapu, D. Kang, S.W. Wagnon, K. Zhang, M. Mehl, M. Monge-Palacios, H. Wang, S.S. Goldsborough, C.K. Westbrook, W.J. Pitz, Kinetic modeling study of surrogate components for gasoline, jet and diesel fuels: C7-C11 methylated aromatics, Proc. Combust. Inst. 37 (2019) 521–529. https://doi.org/10.1016/j.proci.2018.08.016.